Structure and magnetic properties of *Ln*MnSbO (*Ln* = La and Ce)

Qiang Zhang,[1,2,*] C. M. N. Kumar,[3,4] Wei Tian,[5] Kevin W. Dennis,[1] Alan I. Goldman,[1,2] and David Vaknin[1,2,†]

[1]*Ames Laboratory, Ames, Iowa 50011, USA*

[2]*Department of Physics and Astronomy, Iowa State University, Ames, Iowa 50011, USA*

[3]*Jülich Centre for Neutron Science (JCNS), Forschungszentrum Jülich GmbH, Outstation at SNS, Oak Ridge National Laboratory, Oak Ridge, Tennessee 37831, USA*

[4]*Chemical and Engineering Materials Division, Oak Ridge National Laboratory, Oak Ridge, Tennessee 37831, USA*

[5]*Quantum Condensed Matter Division, Oak Ridge National Laboratory, Oak Ridge, Tennessee 37831, USA*

(Received 14 December 2015; published 11 March 2016)

A neutron powder diffraction (NPD) study of *Ln*MnSbO (*Ln* = La or Ce) reveals differences between the magnetic ground state of the two compounds due to the strong Ce-Mn coupling compared to La-Mn. The two compounds adopt the *P*4/*nmm* space group down to 2 K, and whereas magnetization measurements do not show obvious anomaly at high temperatures, NPD reveals a C-type antiferromagnetic (AFM) order below $T_N = 255$ K for LaMnSbO and 240 K for CeMnSbO. While the magnetic structure of LaMnSbO is preserved to base temperature, a sharp transition at $T_{SR} = 4.5$ K is observed in CeMnSbO due to a spin-reorientation (SR) transition of the Mn^{2+} magnetic moments from pointing along the *c* axis to the *ab* plane. The SR transition in CeMnSbO is accompanied by a simultaneous long-range AFM ordering of the Ce moments, which indicates that the Mn SR transition is driven by the Ce-Mn coupling. The ordered moments are found to be somewhat smaller than those expected for Mn^{2+} ($S = 5/2$) in insulators, but large enough to suggest that these compounds belong to the class of local-moment antiferromagnets. The lower T_N found in these two compounds compared to the As-based counterparts ($T_N = 317$ for LaMnAsO, $T_N = 347$ K for CeMnAsO) indicates that the Mn-*Pn* (*Pn* = As or Sb) hybridization that mediates the superexchange Mn-*Pn*-Mn coupling is weaker for the Sb-based compounds.

DOI: 10.1103/PhysRevB.93.094413

I. INTRODUCTION

Spin and orbital degrees of freedom of transition-metal (*T* = Fe, Co, Mn, ...) pnictide-based compounds such as AT_2As_2 (*A* = Ba, Sr, Ca, ...) or *RT*AsO (*R* = rare-earth elements) settle into distinct ordered magnetic ground states in which for some, especially the Fe-based pnictides, slight doping or external pressure suppresses the static magnetic structure and induces superconductivity [1–3]. In all of these systems, the transition-metal atoms form a square lattice (or are slightly distorted into a rectangular lattice) with a corrugated layer of nearest-neighbor (NN) pnictides (*Pn* = P, As, Sb, Bi) that mediate extended superexchange coupling among the transition metals. The ground state for the parent "1111" and "122" Fe-based pnictides is almost without exception a spin-stripe antiferromagnetic (AFM) plane with varying interplanar stacking that depends on the details of the elements separating the FeAs planes [4,5]. On the other hand, the Co-based pnictides tend to form ferromagnetic (FM) planes, which are static (i.e., $CaCo_{1.86}As_2$) [6] or dynamic (i.e., $SrCo_2As_2$) [7]. It is by now understood that both the Fe- and Co-based "122" family of pnictide compounds exhibit relatively strong AFM next-NN (NNN) exchange coupling (J_2) that, due to its competition with the NN coupling (J_1; $J_1 \sim J_2$), leads to the stripelike magnetic structure or to fluctuations with the same motif. The relatively strong J_1 is intimately related to strong hybridization of *p* and *d* orbitals of *Pn* and *T*, respectively [8–11]. By contrast, Mn-based "1111" pnictides *Ln*MnAsO (*Ln* = La, Nd, Ce) tend to undergo a simple checkerboard (C-type) AFM structure [12–14] with much higher transition temperatures than their Fe-based counterparts, indicating effectively stronger NN interaction, i.e., $J_1 > 2J_2$. A neutron powder diffraction (NPD) study of the isostructural PrMnSbO has shown similar C-type Mn magnetic ordering below $T_N \approx 230$ K, followed by a spin reorientation (SR) to the *ab* plane [15]. In addition, a tetragonal-to-orthorhombic transition at low temperatures was found at ~35 K, presumably due to the Pr 4*f* electron degree of freedom. It is interesting to note that this variable magnetic behavior of transition-metal pnictides (i.e., AT_2Pn_2 or *RTPn*O) is strikingly different than that of other insulating transition-metal oxides. For instance, the Li orthophosphate family $LiTPO_4$ (*T* = Mn, Fe, Co, and Ni) all exhibit the same AFM ground state that differs only in the direction of the ordered moment, and the moment size to a good degree of accuracy obeys the classical Hund's rules under a crystal-field effect as a local moment [16–18]. In fact, the average moment size for transition-metal pnictides tends to be significantly smaller than the local moment in insulators, suggesting a high degree of itineracy in the *d* shell and an instability of the electronic structure.

Here, we report on the preparation, structure, and magnetic properties of LaMnSbO and CeMnSbO by employing neutron diffraction techniques and bulk magnetization measurements. Room-temperature structures of these two compounds have been reported [19]. Although both systems are expected to exhibit similar properties in the MnSb triple plane, the presence of Ce or another magnetic rare-earth element has been shown to have an effect on the nuclear structure and the magnetic structure of the transition metal [12,14,15,20]. These Sb-based

*qzhangemail@gmail.com

†vaknin@ameslab.gov

 ©2016 American Physical Society

pnictides are also instructive in systematically examining the effect of the of As-Sb replacement in LnMnPnO.

II. EXPERIMENTAL DETAILS

The synthesis of the polycrystalline LaMnSbO compound is similar to that reported by Schellenberge *et al.* [19]. Two starting materials, MnO and LaSb, were mixed thoroughly in stoichiometric proportions (LaSb was prepared first by reacting La and Sb powders at 600 °C for 5 h and subsequently at 950 °C for 12 h under 1/3 atm of argon). The mixed powder was sealed in a tantalum tube under argon at 1/3 atm and sintered at 1120 °C for 24 h. The CeMnSbO was prepared in one step using Ce, Sb, and MnO as starting materials by mixing them thoroughly, sealing the mixture in a quartz tube under 1/3 atm of argon, and sintering at 1120 °C for 24 h. All mixing and thorough grinding of the starting materials were conducted under an inert environment (i.e., glove box under argon) to minimize metal oxidation. Magnetization measurements were carried out in a superconducting quantum interference device (Quantum Design MPMS-7S, SQUID) magnetometer. Neutron powder diffraction (NPD) measurements on ≈4 g LaMnSbO and CeMnSbO samples were conducted on the HB1A triple-axis spectrometer with a fixed-incident energy of 14.6 meV [located at the High Flux Isotope Reactor (HFIR) at the Oak Ridge National Laboratory]. The measurements on HB1A were performed with a highly oriented pyrolytic graphite stack (HOPG) analyzer to yield a lower background scattering (providing approximately 1 meV energy resolution). Two HOPG crystals were used to filter out the $\lambda/2$ component from the incident beam. The data between $2 < T < 300$ K of LnMnSbO (La and Ce) were collected using an *orange* cryostat, whereas a high-temperature furnace was used for the measurements for CeMnSbO between $300 < T < 670$ K.

Neutron powder diffraction (NPD) measurements were also performed on the time-of-flight (TOF) powder diffractometer, POWGEN, located at the Spallation Neutron Source at Oak Ridge National Laboratory. The data were collected with neutrons of central wavelengths 1.333 and 3.731 Å, covering the d-spacing range 0.4–6 and 1.65–14 Å, respectively. About 2.5 g samples were loaded in a vanadium container of 8 mm diameter and measured in an orange cryostat in the temperature range of 2–300 K. All of the neutron diffraction data were analyzed using the Rietveld refinement program FULLPROF suite [21].

III. RESULTS AND DISCUSSION

Figure 1 shows neutron powder diffraction scans of LaMnSbO and of CeMnSbO measured on HB1A above their AFM transition temperatures. The solid lines are the best calculated intensities based on the ZrCuSiAs-type $P4/nmm$ space group consistent with previous powder x-ray diffraction reports [19] (note that the measurement and refinement include peaks from an Al sample can). The refinement of the CeMnSbO indicates that there is a small amount of MnSb present in the sample as an impurity phase. Both LaMnSbO and CeMnSbO maintain tetragonal $P4/nmm$ symmetry to the lowest temperature, namely, 2 K, as summarized in Table I. A three-dimensional (3D) graphic representation of the crystals,

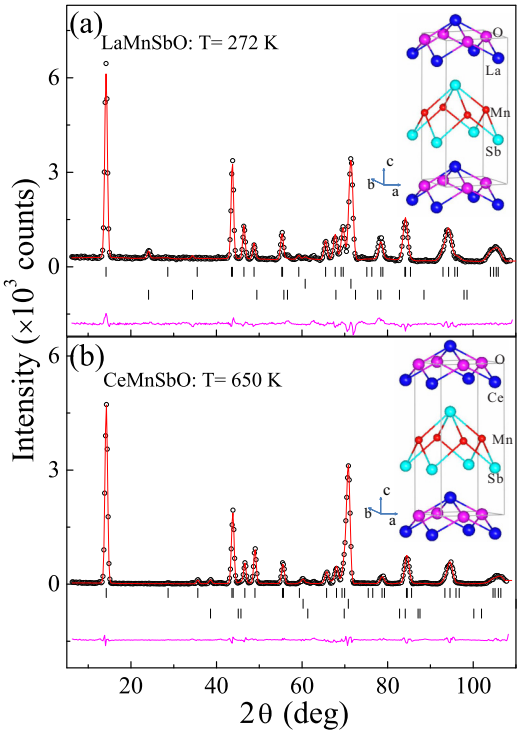

FIG. 1. Neutron diffraction patterns measured on HB1A (a) at 272 K for LaMnSbO and (b) at 650 K for CeMnSbO. The insets show the corresponding graphic representation of the crystal structure. The blue spheres indicate (a) La and (b) Ce atoms. The observed data and the Rietveld fit are indicated by the open circles and solid lines, respectively, with the difference curve at the bottom. The vertical bars mark the positions of Bragg reflections for the expected "ZrCuSiAs"-type structure (top), and the Al sample holder and impurity phase of Sb in LaMnSbO and MnSb in CeMnSbO (bottom).

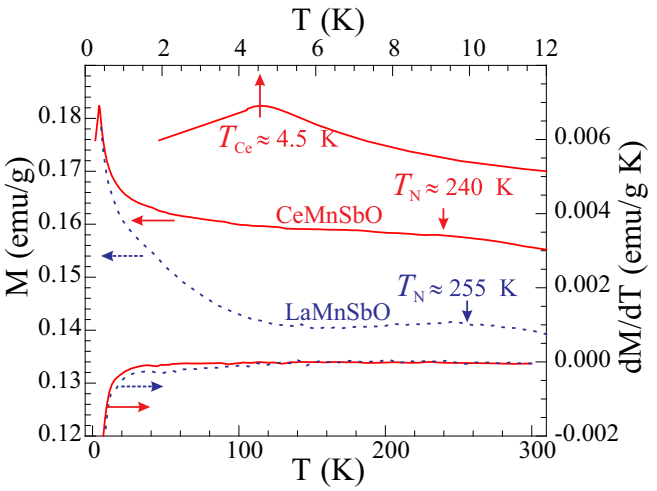

FIG. 2. Temperature dependence of the magnetization of LaMnSbO and CeMnSbO at applied magnetic of 0.01 T. The two lowest curves (dashed and solid lines) show the derivatives of the magnetization for both samples with respect to temperature. Note that both curves do not show anomalies at the AFM transition of Mn at around 250 K; however, a sharp peak associated with the Mn spin reorientation and Ce ordering is observed at $T_{SR} = T_{CE} \approx 4.5$ K.

TABLE I. Structural and magnetic data corresponding to simultaneous crystal and magnetic structure refinements of CeMnAsO, CsMnSbO, and LaMnSbO at a few representative temperatures. All of the refinements were carried out with the space group $P4/nmm$ in tetragonal symmetry. Refined results obtained from the measurements at HB1A are indicated by HB1A; otherwise the data corresponds to the results obtained from the measurements at POWGEN. The values in parenthesis represent the estimated 'standard deviations' in the last digit(s).

		CeMnSbO			LaMnSbO			CeMnAsO	
	T (K)	300	15	2	272(HB1A)	1.5(HB1A)	300	48	2
Unit cell parameters									
a (Å)		4.2104(1)	4.2003(1)	4.2003(1)	4.247(1)	4.236(1)	4.0914(3)	4.0826(3)	4.0826(1)
c (Å)		9.5034(2)	9.4774(3)	9.4752(3)	9.572(2)	9.545(2)	8.9701(7)	8.9480(2)	8.9452(3)
V (Å^3)		168.47(1)	167.21(1)	167.17(1)	172.61(6)	171.25(5)	150.15(1)	149.15(1)	149.09(1)
Atoms (Wyckoff site)									
Ce-La (2c)	z	0.1186(7)	0.1171(6)	0.1195(5)	0.115(2)	0.116(2)	0.1322(6)	0.1322(2)	0.1328(5)
	$B_{\rm iso}$ (Å^2)	0.665(70)	0.308(87)	0.315(84)	0.3(2)	0.1(3)	0.17(9)	0.09(3)	0.07(5)
	$m(\mu_{\rm B})$			1.02(4)					1.08(4)
Mn (2b)	$B_{\rm iso}$ (Å^2)	1.1(2)	0.41(10)	0.322(78)	2.0(4)	2.0(5)	0.42(1)	0.195(30)	0.161(61)
	$m(\mu_{\rm B})$		3.73(4)	3.92(4)		3.45(6)	2.60(5)	3.41(3)	4.18(4)
As-Sb (2c)	z	0.6827(5)	0.6820(5)	0.6818(4)	0.674(1)	0.675(2)	0.6716(5)	0.6712(2)	0.6704(4)
	$B_{\rm iso}$ (Å^2)	0.823(35)	0.259(66)	0.223(6)	3.5(4)	3.1(6)	0.42(8)	0.18(3)	0.17(5)
O (2a)	$B_{\rm iso}$ (Å^2)	0.63(4)	0.41(8)	0.37(1)	0.6(3)	0.2(4)	0.29(8)	0.20(3)	0.24(5)
Bond length									
	Mn-Sb	2.729(3)	2.718(3)	2.716(2)	2.700(7)	2.695(8)	2.557(3)		
	Mn-As							2.5542(9)	2.548(2)
	Ce-O	2.388(3)	2.386(3)	2.385(2)				2.359(1)	2.362(2)
Distance of NN ions									
	Mn-Mn	2.9772(1)	2.9701(1)	2.9701(1)	3.0029(5)	2.9950(3)		2.8868(2)	2.8868(1)
	Ce-Ce (ab plane)	4.2104(1)	4.2003(1)	4.2003(1)				4.0826(1)	4.0826(1)
	Ce-Ce (along c)	3.734(6)	3.735(5)	3.731(4)				3.7324(2)	3.739(4)
	Ce-Mn (along c)	4.192(6)	4.173(5)	4.175(4)				3.875(4)	3.868(4)
Discrepancy factors									
	χ^2	1.45	1.14	1.48	2.32	3.07	2.68	1.88	2.19
	R_p (%)	5.04	7.00	6.2	10.9	11.9	5.27	5.91	6.89
	R_{wp}(%)	7.04	10.04	8.75	11.6	12.5	8.48	9.46	10.8
	$R_{\rm mag}$(%)		8.76	6.97		13.3	7.28	3.12	6.07

based on our Rietveld analysis, is included as insets in Fig. 1. Figure 2 shows the magnetization measurements of LaMnSbO and CeMnSbO and their derivatives with respect to temperature in the temperature range of 2–300 K. The CeMnSbO exhibits a sharp peak at $T \approx 4.5$ K which, as we demonstrate below, is due to Ce ordering and Mn internal spin flop similar to that observed in CeMnAsO [14] (spin flop and spin reorientation by 90 degrees are used interchangeably throughout). It is interesting to note that both compounds do not show obvious features in the susceptibilities or their derivatives to indicate a transition from a paramagnetic to a magnetically ordered state. However, neutron diffraction patterns at low scattering angles (2θ) show intensity in the forbidden (100) reflection and significant change in intensities of the (101) and (002) reflections (see Fig. 3), indicating the ordering of the Mn sublattice.

Figure 4 shows the integrated intensities of the (100) and (101) magnetic Bragg reflections as a function of temperature representing the square of the sublattice magnetic order parameters for both samples. Fitting the order parameters to a power law, $I(T) = a(1 - T/T_{\rm N})^{2\beta} + b$, yields $T_{\rm N} = 255 \pm 5$ K and $\beta = 0.25(3)$ for LaMnSbO and $T_{\rm N} = 240 \pm 4$ K and $\beta = 0.24(3)$ for CeMnSbO. These values are very similar to that obtained for CeMnAsO [14,22]. Such phenomenological power-law behavior over the extended range of temperatures with similar exponents has been explained for similar quasi-2D systems [23,24] that possess in-plane exchange coupling J_1 that is significantly stronger than the interlayer one, $J_c/J_1 \ll 1$ [25]. The quasi-2D behavior extracted from the order parameter is intimately consistent with the absence of clear AFM signatures in the aforementioned susceptibility. The absence of clear anomaly at or near $T_{\rm N}$ in the susceptibility is indicative of the two-dimensional nature of the spin system, namely, strong in-plane spin-spin coupling (J_1) and very weak interplanar coupling with likely large but fluctuating spin correlations above $T_{\rm N}$. This suggests that the transition temperature $T_{\rm N}$ does not represent the energy scale of nearest-neighbor (NN) coupling J_1, i.e., $J_1 \gg k_B T_{\rm N}$.

As the temperature is lowered below $T_{\rm N}$, the intensities of the (100) and the (101) for LaMnSbO saturate at base temperature [see Fig. 3(a)], indicating that no further magnetic or structural transitions occur below $T_{\rm N}$. The Rietveld fit to the NPD pattern at 1.5 K in LaMnSbO and analysis by SARAh [26] reveal that the Mn spins form a nearest-neighbor antiferromagnetic alignment in the ab plane and ferromagnetic alignment along the c axis (C-type AFM order) with moment

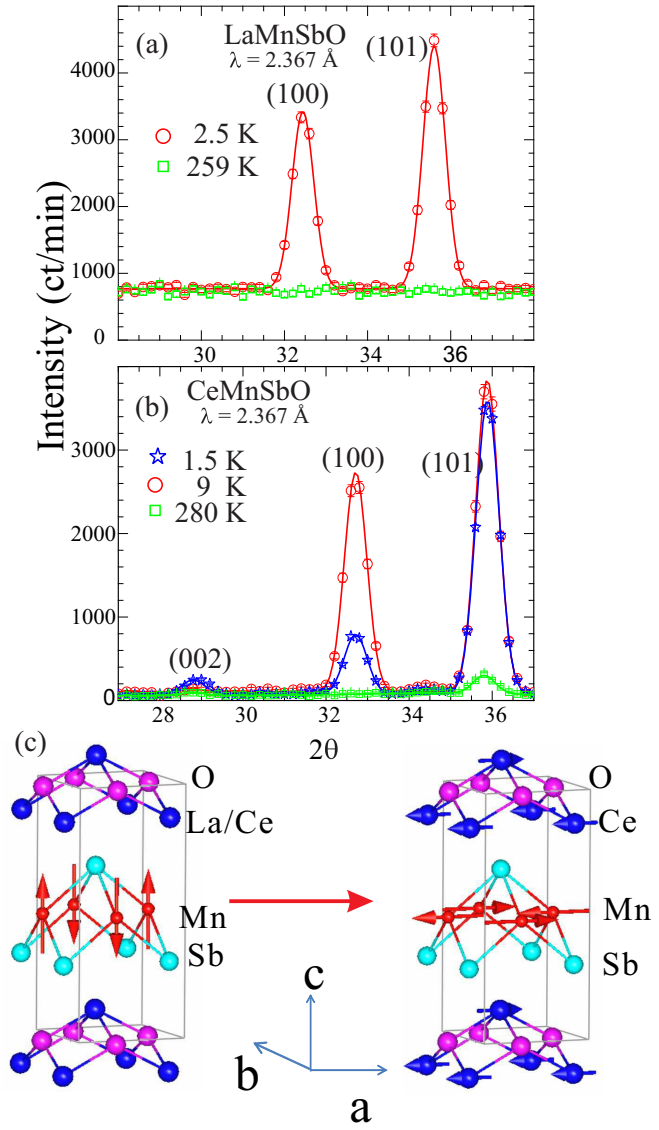

FIG. 3. (a) Low-angle neutron diffraction scans showing the emergence of the (100) and the increase in intensity (101) reflections for (a) LaMnSbO and (b) CeMnSbO due to a simple Mn AFM ordering (checkerboardlike) as shown in the left part of (c). For CeMnSbO, as the temperature is lowered further (below ≈4.5 K), the (100) Bragg reflection is significantly reduced in intensity and simultaneously the (200) gains intensity, indicating a uniform spin flop of the Mn moments from pointing along the c axis to pointing in the ab plane and the emergence of Ce ordering with a magnetic structure, as depicted in the right side of (c).

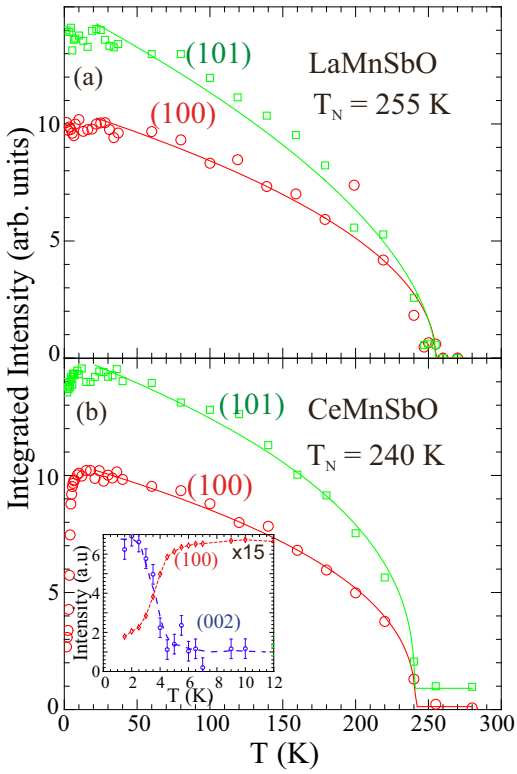

FIG. 4. Integrated intensities vs temperature of the (100) and (101) Bragg peaks for (a) CeMnSbO and (b) LaMnSbO with a fit to a power law (solid lines). At low temperatures, the (100) peak of CeMnSbO shows a strong reduction in intensity around $T_{SR} = 4.5$ K.

along the c axis as shown in Fig. 3(c) (left panel). However, as shown in Fig. 3(b) for CeMnSbO below $T \approx 4.5$ K, there is a dramatic decrease in the intensity of the (100) and a lesser decrease in the (101). In addition, Fig. 3(b) also shows a moderate increase in the (002) peak (more details of its temperature dependence can be found in the inset of Fig. 4(b)). Representation analysis by SARAh and detailed Rietveld fit to the whole diffraction patterns at 40 and 1.5 K indicate that below ∼4.5 K, the Mn spins undergo an internal spin-flop transition in unison from pointing along the crystallographic c axis into the plane [the main evidence is the behavior of the (100) reflection] while keeping the C-type AFM order. And, simultaneously, the AFM ordering of the Ce ions occurs where Ce spins are ferromagnetically aligned in the ab plane and antiferromagnetically between planes [see Fig. 3(c)]. The main indicator for the Ce ordering is the abrupt increase in the intensity of the (002) reflection [see inset in Fig. 4(b)]. The spin-flop transition is not observed in LaMnSbO involving the nonmagnetic La, but is found in CeMnSbO, which is evidence that the transition is driven by Ce-Mn coupling. The ordering of the Ce spins in the ab plane indicates a finite single-ion anisotropy for the Ce spin due to its orbital degree of freedom ($L = 3$) that in this case orients the Ce moment in the basal plane and forces the Mn ions, with the very weak or no single-ion anisotropy ($L = 0$) to follow with spin reorientation to the ab plane via Ce-Mn coupling.

The average ordered Mn moments of LaMnSbO and CeMnSbO at ≈2 K are found to be 3.45(6) and 3.92(4)μ_B, respectively, both of which are lower than 5μ_B expected for Mn^{2+} in insulators, but large enough to primarily be considered as local moments. The checkerboardlike AFM structure of the C-type order in both compounds below T_N suggests that the NN interaction J_1 is more dominant compared to the NNN J_2. Although their magnetic behaviors are similar to those in LnMnAsO (Ln = La and Ce), the Sb-based counterparts differ in three distinct respects: (1) The transition temperatures, $T_N = 317$ K [13] for LaMnAsO and 347 K for CeMnAsO [14], are found to be lower

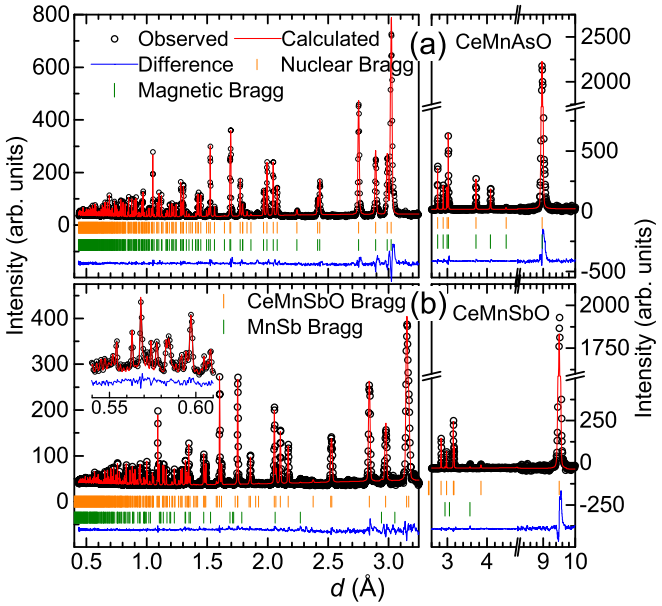

FIG. 5. Observed (measured on POWGEN) and calculated diffraction patterns and their difference for (a) CeMnAsO and (b) CeMnSbO at 300 K. The left and right frames correspond to the data collected with center wavelengths 1.333 and 3.731 Å, respectively. Note that at 300 K, CeMnAsO is AFM showing extra reflections that are also accounted for in the calculations. The inset in (b) shows the high quality of the POWGEN data and the calculated fit at the high-order reflections region.

by almost 100 K for LaMnSbO and CeMnSbO. (2) The spin-reorientation transition observed at ≈35 K in CeMnAsO is suppressed to ≈4.5 K in CeMnSbO. (3) The third magnetic transition at $T^* \approx 7$ K in CeMnAsO [14], possibly related to a collinear-to-noncollinear magnetic structure, is absent in CeMnSbO, implying that the magnetic ground states of CeMnAsO and CeMnSbO are different. These differences indicate an appreciable effect of the As-by-Sb substitution on the magnetism of LnMnPnO (Pn = As or Sb). To shed more light on these differences, we have employed POWGEN to systematically study CeMnAsO and CeMnSbO and compare their structure and magnetism in detail, taking advantage of the superior instrumental resolution of POWGEN over that of HB1A, and also the wider Q range (or d-spacing range) that it covers. For comparison, Fig. 5 shows the TOF powder diffraction patterns from CeMnAsO and CeMnSbO at $T = 300$ K. Both figures also include the best calculated fit to the diffraction patterns that at the large d spacing include magnetic peaks for CeMnAsO present at 300 K, as this system orders at $T_N = 347$ K [14]. The high quality of the POWGEN data and the calculated fit at the high-order reflections region are demonstrated in the inset of Fig. 5(b). Table I lists the best-fit parameters to the diffraction patterns at selected temperatures that represent the various phases of the two systems, in accordance with the magnetic models described above. For both systems, we find that the average magnetic moment of Ce is consistently on the order of $1\mu_B$, whereas the expected value for the free ion is $g(JLS)J = 2.1\mu_B$ for the $4f^1$ configuration of Ce^{3+} [$g(JLS)$ is the Landé g factor]. This suggests that crystal-field effects play a role in adjusting the actual magnetic moment, an issue that can be further explored by spectroscopic methods.

Also listed in Table I are the bond lengths of As-Mn and Sb-Mn at selected temperatures. Consistently, the Sb-Mn bond length is significantly longer than that of the As-Mn bond, which could account for the significantly lower T_N presumably due to a lesser p-d hybridization of Pn and Mn that results in a weaker superexchange Mn-Mn coupling J_1 in the SbMn plane. The reduced T_{SR} in CeMnSbO implies weaker Ce-Ce and Ce-Mn interactions than those in CeMnAsO. Note that in both CeMnAsO and CeMnSbO, each square sheet of O^{2-} ions is sandwiched between two square sheets of Ce^{3+} ions to form a R-O-R slab and alternates with the Pn-Mn-Pn slab along the c axis. Ce^{3+} ions above and below the square sheet of the Mn^{2+} form a Mn_4Ce square pyramid and the superexchange AFM Ce-Ce interaction along the c axis is mediated by O atoms. As shown in Table I, the longer Ce-O bond length in CeMnSbO is probably related to the weaker AFM superexchange Ce-Ce interaction in CeMnSbO along the c axis. As for the Ce-Mn interactions, density functional theory (DFT) calculations of CeMnAsO show that they can be complicated due to the presence of multiple interactions, such as the Heisenberg, Dzyaloshinskii-Moriya (DM), and biquadratic (BQ) exchange interactions in order of strength. Thus, the DM (stronger than the BQ) leads to a noncollinear magnetic structure ground state with the Mn moments orthogonal to those of the Ce moments [27]. Note that the NPD is not sufficient in distinguishing the collinear from the noncollinear arrangement between Ce^{3+} and Mn^{2+} moments in CeMnSbO or in CeMnAsO. However, susceptibility measurements and a very weak change in intensity of the (002) magnetic peak at T^* have been observed for CeMnAsO and have been associated with the collinear-to-noncollinear transition [14]. Considering the much lower T_{SR} in CeMnSbO, magnetization measurements below ∼1 K and further DFT calculations may shed more light on the issue of the ground state of CeMnSbO. Nevertheless, the weaker total Ce-Mn interaction in CeMnSbO is most likely related to the larger distance between the two NNs (along the c axis) compared to that in the CeMnAsO, as shown in Table I.

The high-resolution d-spacing available by the TOF POWGEN compared to HB1A yields cell parameters with a high relative accuracy as a function of temperature (i.e., excluding any systematic error that is temperature independent). As shown in Fig. 6, such high resolution allows detection of a magnetoelastic effect that manifests itself in an anomaly in the c/a ratio of the cell parameters as a function of temperature, with an onset at T_{SR} of the spin-reorientation transition and Ce ordering for CeMnAsO and for CeMnSbO. In contrast, the cell volume of both compounds monotonically decreases with decreasing temperature without anomaly at T_{SR}.

In addition to inducing spin flop in LnMnSbO, the rare-earth element has an effect on the lattice. Whereas a T-O transition is observed in PrMnSbO at 35 K [15], the tetragonal structure in LaMnSbO and CeMnSbO is preserved to the lowest temperature (∼2 K). Kimber *et al.* [15] have proposed that the T-O structural transition in PrMnSbO is driven by the $4f$ electron degrees of freedom in connection to multipolar order of the $4f^2$ electrons of Pr^{3+}. Multipolar ordering of $4f$ electrons has been discussed in more detail in regard to

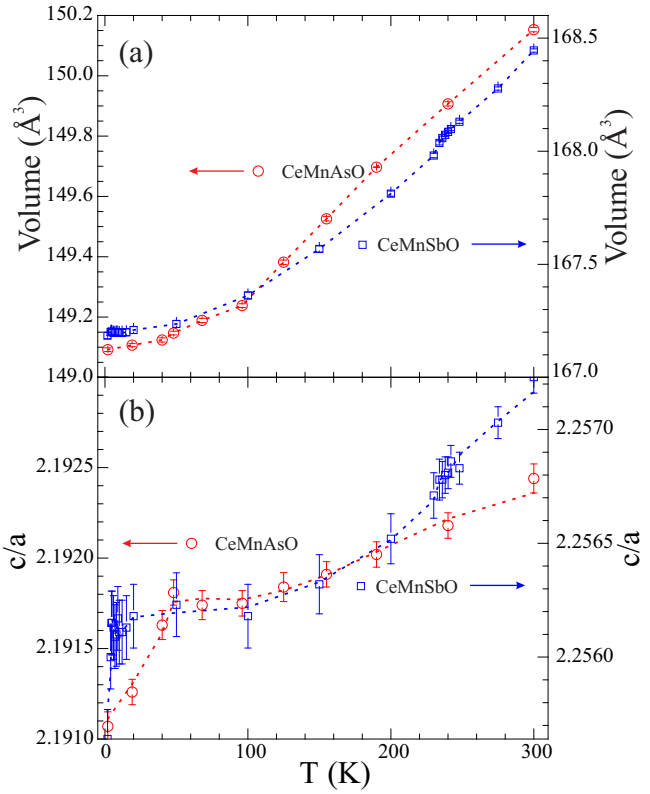

FIG. 6. (a) Temperature dependence of cell volumes for CeMnSbO and CeMnAsO. (b) The c/a ratio of cell parameters showing the magnetoelastic effect at the Ce ordering, $T_{Ce} \approx 4.5$ K for CeMnSbO and ≈35 K for CeMnAsO. Dotted lines are guides to the eye.

various transitions in Pr- and Ce-based compounds [28–32]. La^{3+} has no $4f$ electrons and no multipolar ordering. Ce^{3+}, with only one f electron ($4f^1$) compared to Pr $4f^2$, may exhibit a very weak multipolar ordering that only induces the c/a anomaly observed at $T_{SR} = 4.5$ K, as shown in Fig. 6. It is interesting to point out that a similar scenario as in CeMnSbO has been suggested for the heavy-fermion metal CeB_6 [31]. Nuclear magnetic resonance and resonant x-ray scattering may shed more light on the different multipolar orders of $4f$ electrons of Ce^{3+} and Pr^{3+} in CeMnSbO and PrMnSbO.

IV. CONCLUSIONS

In summary, we report neutron diffraction and magnetization studies on LaMnSbO and CeMnSbO and compare them to other isostructural systems. The main conclusions from our results are as follows: (1) The Mn^{2+} moments order in a simple AFM checkerboardlike (C-type) structure with the moments along the c axis, with no indication of a transition in the magnetization as a function of temperature. This and the order-parameter behavior as a function of temperature indicate that the interplanar coupling is very weak compared to the in-plane coupling, implying a quasi-2D behavior of the magnetic system, and that the NN coupling J_1 is likely much larger than $k_B T_N$. (2) The extracted average magnetic moment at base temperatures ($\sim 4\mu_B$) is relatively large and very close to the value expected from a Mn^{2+} ($\sim 5\mu_B$) with $S = 5/2$. The small reduction from the value expected in insulators implies very weak itineracy in the d shell and that to a good approximation in these systems the Mn spin behaves more like a local moment. (3) The coupling of Ce-Mn is sufficiently strong to alter the orientation of the magnetic moments from pointing along the c axis to the ab plane at $T_{SR} = 4.5(5)$ K. At the same temperature, the Ce moments undergo AFM ordering at $T_{Ce} = T_{SR}$. We regard this transition as an internal spin-flop transition similar to the magnetic-field-induced spin-flop transition commonly observed in Mn-based insulators [18] due to the weak (or no) spin-orbit coupling (angular momentum $L \sim 0$ for Mn^{2+} ion) that tends to result in very weak single-ion anisotropy such that the spins readily flop by external or internal magnetic fields. (4) The significantly lower Mn ordering temperatures ($T_N \sim 250$ K) of the Sb-based compared to the higher ones for As-based compounds ($T_N \sim 350$ K) imply stronger NN coupling J_1 in the latter, suggesting a weaker p-d hybridization in Sb-Mn compared to As-Mn. (5) The replacement of As by Sb lowers T_{SR} and suppresses the noncollinear transition (seen at $T^* = 7$ K in CeMnAsO), indicating weaker Ce-Ce interactions in CeMnSbO. (6) In contrast to PrMnSbO which undergoes a transition to an orthorhombic phase at low temperatures due to Pr^{3+} $4f^2$ multipolar effects, the chemical structure of LaMnSbO and CeMnSbO is preserved to the lowest temperature (~2 K), suggesting a lesser multipolar effect in Ce^{3+} $4f^1$ that only induces a magnetoelastic anomaly observed in the c/a lattice parameters as a function of temperature, while, as expected, even the magnetoelastic anomaly is absent for the nonmagnetic $La^{3+}(4f^0)$.

ACKNOWLEDGMENTS

Research at Ames Laboratory is supported by the U.S. Department of Energy, Office of Basic Energy Sciences, Division of Materials Sciences and Engineering under Contract No. DE-AC02-07CH11358. Use of the High Flux Isotope Reactor and the Spallation Neutron Source at the Oak Ridge National Laboratory is supported by the U.S. Department of Energy, Office of Basic Energy Sciences, Scientific Users Facilities Division.

[1] D. C. Johnston, Adv. Phys. **59**, 803 (2010).
[2] M. D. Lumsden and A. D. Christianson, J. Phys.: Condens. Matter **22**, 203203 (2010).
[3] P. Dai, Rev. Mod. Phys. **87**, 855 (2015).
[4] Q. Huang, Y. Qiu, W. Bao, M. A. Green, J. W. Lynn, Y. C. Gasparovic, T. Wu, G. Wu, and X. H. Chen, Phys. Rev. Lett. **101**, 257003 (2008).
[5] C. de la Cruz, Q. Huang, J. W. Lynn, J. Li, W. Ratcliff II, J. L. Zarestky, H. A. Mook, G. F. Chen, J. L. Luo, N. L. Wang, and P. Dai, Nature (London) **453**, 899 (2008).
[6] D. G. Quirinale, V. K. Anand, M. G. Kim, A. Pandey, A. Huq, P. W. Stephens, T. W. Heitmann, A. Kreyssig, R. J. McQueeney, D. C. Johnston, and A. I. Goldman, Phys. Rev. B **88**, 174420 (2013).

[7] W. Jayasekara, Y. Lee, A. Pandey, G. S. Tucker, A. Sapkota, J. Lamsal, S. Calder, D. L. Abernathy, J. L. Niedziela, B. N. Harmon, A. Kreyssig, D. Vaknin, D. C. Johnston, A. I. Goldman, and R. J. McQueeney, Phys. Rev. Lett. **111**, 157001 (2013).
[8] F. Ma, Z.-Y. Lu, and T. Xiang, Phys. Rev. B **78**, 224517 (2008).
[9] K. Haule and G. Kotliar, New J. Phys. **11**, 025021 (2009).
[10] Y. Lee, D. Vaknin, H. Li, W. Tian, J. L. Zarestky, N. Ni, S. L. Bud'ko, P. C. Canfield, R. J. McQueeney, and B. N. Harmon, Phys. Rev. B **81**, 060406 (2010).
[11] T. Yildirim, Phys. Rev. Lett. **102**, 037003 (2009).
[12] A. Marcinkova, T. C. Hansen, C. Curfs, S. Margadonna, and J.-W. G. Bos, Phys. Rev. B **82**, 174438 (2010).
[13] N. Emery, E. J. Wildman, J. M. S. Skakle, A. C. Mclaughlin, R. I. Smith, and A. N. Fitch, Phys. Rev. B **83**, 144429 (2011).
[14] Q. Zhang, W. Tian, S. G. Peterson, K. W. Dennis, and D. Vaknin, Phys. Rev. B **91**, 064418 (2015).
[15] S. A. J. Kimber, A. H. Hill, Y.-Z. Zhang, H. O. Jeschke, R. Valentí, C. Ritter, I. Schellenberg, W. Hermes, R. Pöttgen, and D. N. Argyriou, Phys. Rev. B **82**, 100412(R) (2010).
[16] R. P. Santoro, D. J. Segal, and R. E. Newnham, J. Phys. Chem. Solids **27**, 1192 (1966).
[17] D. Vaknin, J. L. Zarestky, J. E. Ostenson, B. C. Chakoumakos, A. Goñi, P. J. Pagliuso, T. Rojo, and G. E. Barberis, Phys. Rev. B **60**, 1100 (1999); D. Vaknin, J. L. Zarestky, L. L. Miller, J.-P. Rivera, and H. Schmid, *ibid.* **65**, 224414 (2002); Phys. Rev. Lett. **92**, 207201 (2004).
[18] R. Toft-Petersen, N. H. Andersen, H. F. Li, J. Li, W. Tian, S. L. Bud'ko, T. B. S. Jensen, C. Niedermayer, M. Laver, O. Zaharko, J. W. Lynn, and D. Vaknin, Phys. Rev. B **85**, 224415 (2012).
[19] I. Schellenberg, T. Nilges, and R. Pöttgen, Z. Naturforsch. **63B**, 834 (2008).
[20] Q. Zhang, W. Tian, H. Li, J.-W. Kim, J. Yan, R. W. McCallum, T. A. Lograsso, J. L. Zarestky, S. L. Bud'ko, R. J. McQueeney, and D. Vaknin, Phys. Rev. B **88**, 174517 (2013).
[21] J. Rodriguez-Carvajal, Physica B **192**, 55 (1993).
[22] We note that in Ref. [14] we quoted $\beta = 0.47$ instead of $\beta = 0.24$.
[23] D. Vaknin, E. Caignol, P. K. Davies, J. E. Fischer, D. C. Johnston, and D. P. Goshorn, Phys. Rev. B **39**, 9122 (1989).
[24] D. Vaknin, S. K. Sinha, C. Stassis, L. L. Miller, and D. C. Johnston, Phys. Rev. B **41**, 1926 (1990).
[25] A. Singh, Z. Tesanovic, H. Tang, G. Xiao, C. L. Chien, and J. C. Walker, Phys. Rev. Lett. **64**, 2571 (1990).
[26] A. S. Wills, Physica B **276–278**, 680 (2000).
[27] C. Lee, E. Kan, H. Xiang, R. K. Kremer, S. Lee, Z. Hiroi, and M. Whangbo, Inorg. Chem. **51**, 6890 (2012).
[28] S. Uma, T. Sarkar, K. Sethupathi, M. Seshasayee, G. Rangarajan, Chen Changkang, Hu Yongle, B. M. Wanklyn, and J. W. Hodby, Phys. Rev. B **53**, 6829 (1996).
[29] A. Kiss and P. Fazekas, J. Phys.: Condens. Matter **15**, S2109 (2003).
[30] H. C. Walker, K. A. McEwen, D. F. McMorrow, M. Bleckmann, J.-G. Park, S. Lee, F. Iga, and D. Mannix, Phys. Rev. B **79**, 054402 (2009).
[31] A. S. Cameron, G. Friemel, and D. S. Inosov, arXiv:1509.03588.
[32] T. Matsumura, T. Yonemura, K. Kunimori, M. Sera, and F. Iga, Phys. Rev. Lett. **103**, 017203 (2009).